Biotribology xxx (xxxx) xxx–xxx

Contents lists available at ScienceDirect

Biotribology

journal homepage: www.elsevier.com/locate/biotri

A Confocal Fluorescence Microscopy Method for Measuring Mucous Layer Growth on Living Corneal Epithelia

Tristan T. Hormel*, Tapomoy Bhattacharjee, Angela A. Pitenis, Juan M. Urueña, W. Gregory Sawyer, Thomas E. Angelini

Department of Mechanical and Aerospace Engineering, University of Florida, Gainesville, FL 32611, United States

ARTICLE INFO

Keywords:
Mucin
Cornea
Monolayer
Epithelium
Tribology
Rheology

ABSTRACT

Mucous layers at corneal epithelial cell surfaces perform a variety of tribological roles and are integral to the function of associated biological structures. The primary component of these layers are mucin glycosylated proteins, a broad and diverse class of biological macromolecules that influence tribological and rheological characteristics of the eye's tear film. The tear film composition is incessantly modulated by environmental conditions, active production by living cells, and passive processes such as degradation or wear. Quantitative investigation of mucin production and accumulation at the corneal surface will improve current understanding of tear film stability and function. Here, we present fluorescence microscopy and image analysis techniques capable of capturing the dynamics of mucous layer growth. Using this technique, we observe a non-monotonically thickening mucin layer at the apical surface of a corneal epithelial cell monolayer, while the total amount of mucin increases at a rate indicative of diffusion limited growth.

1. Introduction

Mucous barriers that coat epithelial surfaces provide protection to cells in many ways. It is frequently noted that mucous layers form an integral part of the immune system by protecting endothelial cells from infection [1], and that they provide a barrier preventing direct environmental damage to cells [2,3]. A more specific and no less important function of mucous layers occurs at the corneal surface [4]. Here, mucins maintain the tear film's tribological and rheological properties [5], both of which can be disrupted by pathologies, such as dry eye, ultimately leading to impaired vision [6,7]. These protective functions are performed at epithelial surfaces where mucous layers are incessantly subject to shear and friction forces.

One consequence of the dynamic environments in which mucous layers are found is that the thickness of the layer fluctuates in time as it is sheared and compressed [8]. For this reason, cells are constantly producing mucin glycoproteins [2], the primary component of mucous layers [9], to replenish those that have been lost in either passive processes, such as diffusion or proteolytic degradation, or in active processes associated with environmental interactions [10]. The growth dynamics of these layers are not well-studied in many contexts, and in particular in the corneal epithelium, where it has previously been problematic to construct epithelial cell lines that adequately mimic *in vivo* mucin production [11]. The development of an *in vitro* method for monitoring the growth, maintenance, and removal of mucin in epithelial monolayers would open a wide frontier of opportunities for studying the protective mechanisms of mucous layers within the controlled laboratory environment and with a diversity of experimental tools.

Here we develop a method for measuring the growth of mucin layers secreted by living cell monolayers while imaging with time-lapse microscopy over extended periods of time. The method involves supplementing cell growth media at very low concentrations with a fluorophore that binds to the carbohydrate domains of mucin polymers. When the fluorophore concentration in the growth media bath is low enough, it is not detected above the background detector noise. However, as it accumulates on the very high molecular weight mucin macromolecules [12], the number of dye molecules within the microscope focal volume at any instant is large enough to generate sufficient fluorescence signal to be imaged. We develop an analysis method for measuring the changing thickness of a mucin layer over time, produced by a human corneal epithelial cell monolayer. By measuring both the layer thickness and the integrated fluorescence intensity, we are able to infer relative changes in mucin concentration as well (Fig. 1).

2. Materials and Methods

Human telomerase-immortalized corneal epithelial (hTCEpi) cells

* Corresponding author.
E-mail address: hormel@ufl.edu (T.T. Hormel).

http://dx.doi.org/10.1016/j.biotri.2017.04.004
Received 18 November 2016; Received in revised form 28 March 2017; Accepted 3 April 2017
2352-5738/ Published by Elsevier Ltd.

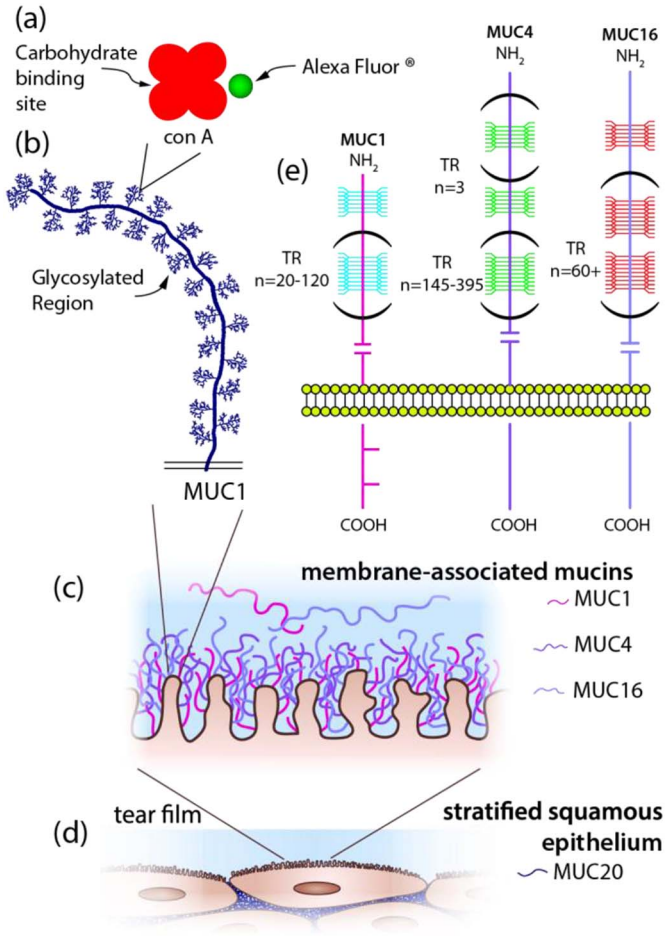

Fig. 1. (Schematic) Fluorescence tagging method and ocular mucins in a biological context. (a) Lectin stain in the form of a Concanavalin A-Alexa Fluor 488 conjugate. Concanavalin A has a width of around 70 Å [13] and four α-D-mannosyl and α-D-glucosyl residue specific binding cites, that bind to oligosaccharides in mucin glycoproteins. (b) Zoom out to a generic mucin to which the lectin stain could bind. Ocular mucins have variable contour lengths, mostly falling between 100 and 600 nm, and persistence lengths of 36 ± 3 nm [14]. (c) Structural motifs of the membrane bound ocular mucins MUC1, MUC4, and MUC16 showing a variable number of tandem repeats (TR) of serine and threonine rich amino acid chains, contributing to variable mucin chain lengths. These regions are O-glycosylated (sugar attached to an amino acid through an oxygen atom). Cleavage cites (=) generate mucins detached from the membrane [15] that can form a mucin rich layer above the surface of the epithelium [16]. (d) Zoom out to the tear film near the corneal epithelial surface, showing both membrane bound and cleaved mucins. (e) Further zoom out, showing corneal epithelial cells in their physiological context.

[17] were grown in KGM-Gold media supplemented with KGM-Gold BulletKit supplements (Lonza, Basel, Switzerland). These cells are known to produce the main membrane-associated ocular mucins (MUC1, MUC4, and MUC16) [18]. All experiments were performed on cells in the same media and in the same environmental conditions (37° C, 5% CO_2). For experiments, confluent islands were plated on fibronectin-coated glass-bottomed culture dishes and allowed to grow overnight. Thirty minutes before use in experiments cells were dyed in 63 nM calcein-red (0.3 μg/mL, ThermoFisher Scientific, Waltham, Massachusetts, USA) and 1.2% DMSO to ensure cells were viable. Immediately prior to imaging cells were then washed to remove any excess calcien-red dye and to remove mucin from cell surfaces. In order to detect mucin production during live cell imaging, the cell growth medium was supplemented with fluorescently tagged Concanavalin-A (ThermoFisher Scientific, Waltham, Massachusetts, USA) at a concentration of 48 nM (molecular weight of 104,000 Da). Concanavalin A binds specifically to internal non-reducing terminal a-D-mannosyl and a-D-glucosyl groups [19]. We captured fluorescence images in three dimensions using Nikon Ti-E inverted microscope with C2 confocal scanning system. Images were captured over a periods of approximately 2 days at 30-minute intervals. Image processing was performed in MATLAB.

3. Results

A slow increase in fluorescence intensity at the monolayer apical surface can be seen directly in snapshots of the cell surface over the two day time-lapse experiments (Fig. 2). We estimate the diffusion coefficient of Concanavalin-A to predict whether this accumulation of fluorescent dye on the monolayer surface is merely diffusion limited adsorption to pre-existing mucin, growth-limited accumulation of mucin with dye arriving rapidly, or some process in between these two limits. To make this estimate of the diffusion coefficient of Concanavilin-A, we use the Stokes-Einstein relation, $D = k_B T/(6\pi\eta R)$, where k_B is Boltzmann's constant, $\eta \approx 1$ mPa s is the cell growth media viscosity, and R is the hydrodynamic radius of Concanavalin-A/Alexa Fluor 488 conjugate, which we approximate to be 7 nm. We find $D \approx 3 \times 10^{-7}\,\mathrm{cm^2\,s^{-1}}$. Under the 48 nM (5 μg/mL) experimental conditions, the average distance between fluorophores in solution is about 300 nm. Thus, at early times, it takes about 3 ms for a fluorophore to find the mucin surface. If the dye has depleted to 1/10 the starting concentration, this time goes up to about 14 ms; when the dye is depleted to 1/1000 the starting concentration, it takes about 300 ms to find the mucin surface. Given that the qualitative time-scale for significant mucin accumulation to be observed is hours to days, or anywhere between 10^3 and 10^6 times longer than these transit times, these experiments fall within the growth-limited regime, far from the diffusion limited regime. We therefore believe that the fluorescence signal in our images, at any instant, serves as a good proxy for the amount of accumulated mucin, and furthermore that any increase in fluorescence intensity is a measure of mucin production.

To analyze mucin growth dynamics, we threshold the confocal 3D stacks using Otsu's method [20], which chooses the intensity cutoff that maximizes the covariance between two sub-populations of voxels (signal and background). In our experiments, this led to between 8% (at the beginning of the time lapse experiment) to 34% (after 24 h) of voxels being counted; these numbers are in accord with our expectations from visual inspection, which also confirmed that the thresholding technique appears to have successfully discriminated between background and signal. Additionally, we employed a multi-level thresholding algorithm which produces the same results. In the thresholded 3D stacks we retain the intensity value of voxels above the threshold

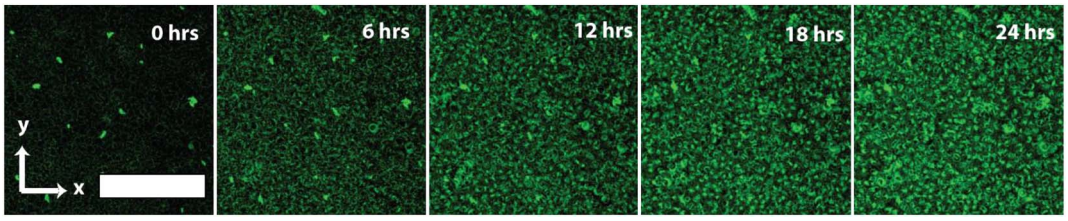

Fig. 2. Growth of a mucin layer at the surface of an hTCEpi cell monolayer over 24 h. At the experimental outset, only small clusters of mucin are visible. After 24 h, mucins coat the surface of every cell. Scale bar: 150 μm.

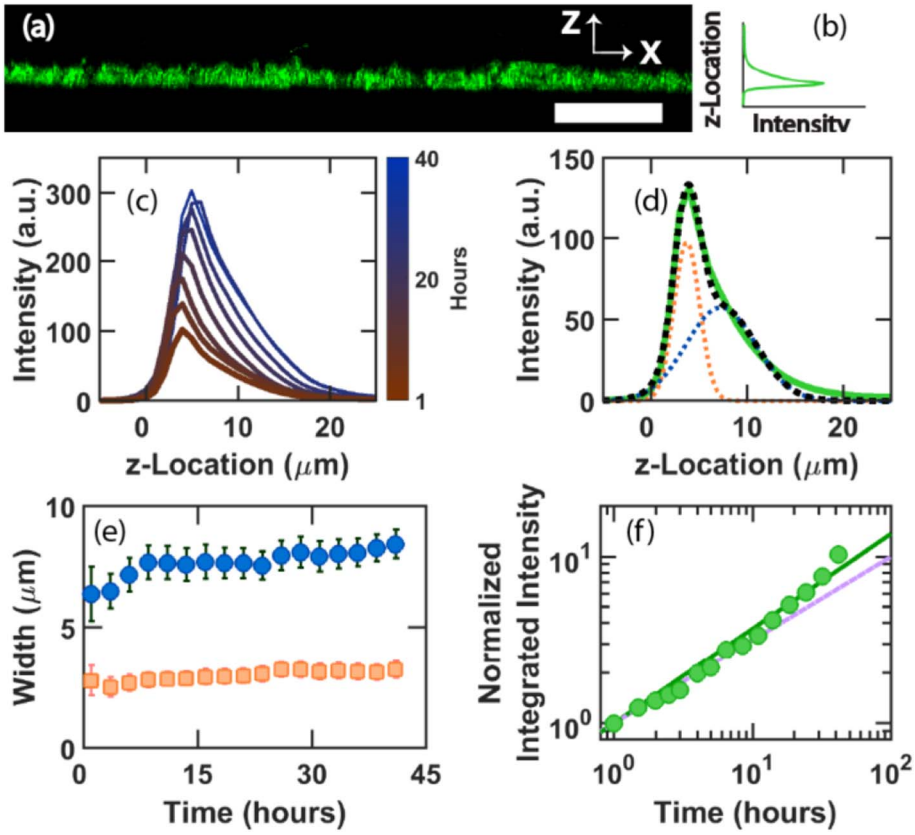

Fig. 3. Mucin production kinetics. (a) Maximum intensity projection into the X-Z plane from a 3D XYZ stack of a mucin coated hTCEpi cell layer. Scale bar: 50 μm. (b) Averaging each 3D XYZ stack along the X and Y directions produces fluorescence intensity profiles along the *Z*-axis, reflecting the average amount of accumulated mucin measured at each vertical position. (c) A time series of fluorescence intensity profiles, flipped perpendicular to the monolayer plane and plotted as a function of z-location. Over time, the amplitude and width of the profiles increase (red to blue color gradations), showing an evolution in the mucin layer. (d) We fit the measured intensity profiles (green) with two Gaussian lineshapes. We find that the leftmost Gaussian measures mucins tightly associated with the cell body (dotted orange trace), while the rightmost corresponds to a mesh of mucins above the monolayer surface (dotted blue trace). The sum of these lineshapes (dotted black line) approximates the measured intensity to a high degree of accuracy. (e) Width of the two Gaussian profiles over time. While the mucous layer above the cell surface thickens over time (blue circles), the membrane associated profile (orange squares) is nearly static in time. Error bars represent 95% confidence intervals for fitted parameters. (f) The integrated intensity of the second Gaussian peak at higher z-locations, normalized to the earliest measurement taken. The green line is power-law fit revealing growth kinetics that resemble diffusion limited behavior, which would scale as a power law with an exponent of ½ (dotted violet line). (For interpretation of the references to color in this figure legend, the reader is referred to the web version of this article.)

level; these values are then averaged along the x- and y-directions, producing fluorescence intensity profiles along the z-axis (Fig. 3a,b). This process is performed on every stack collected in time-lapse, producing a family of fluorescence intensity profiles that show the time-evolution of mucin growth and accumulation in the monolayer (Fig. 3c). The fluorescence profiles possess a sharp peak near the petri dish surface that does not shift along the z-axis in time, and a broad shoulder at larger z-locations which appears to shift away from the petri-dish surface over time (Fig. 3c). Both the sharp peak at low z-locations and the broad peak at high z-locations increase in intensity over time, as expected from the micrographs shown in Fig. 2. These two features in the fluorescence intensity profile appear to correspond to the cell body at low z-locations, and the growing mucin layer at larger z-locations.

To further investigate the two features observed in the fluorescence intensity profiles, and test whether they correspond to the cell bodies and the mucin layer on their apical surface, we perform non-linear least squares curve fitting to extract the integrated intensities and widths of the two features. Qualitatively, the fluorescence intensity profiles look like the sum of a sharp, intense peak and a broad, weak peak. We therefore fit the intensity profiles with two Gaussian lineshapes (Fig. 3d). We do not intend to connect the chosen functional form to any specific model of cell shape or mucin distribution- although models for processes such as diffusion-limited aggregation may be appropriate in our experiments, they would be difficult to apply in this context since we do not directly measure either an absolute quantity of mucin glycoproteins or thickness of the mucous layer. We also do not intend to suggest that the chosen mathematical form is the only one capable of fitting the data, or even that it would be the closest fit. For instance, the actual fluorescence measurement clearly contains some amount of skew about the peak. Instead we use these Gaussian lineshapes as a way to extract changes in peak-width and intensity in a systematic manner such that we obtain a good compromise between quality of fit and easily interpretable results. We find that, with this approach, the quality of fit to fluorescence measurements is very high with $R^2 = 0.99$, and, perhaps just as importantly, the 95% confidence intervals of the individual fitting parameters are very low (displayed as errorbars in Fig. 3e).

If the peak centered at low z-locations arises from fluorescing mucin tightly associated with the cell bodies, it should correspond in width to the known thickness of the monolayer and should not move or broaden significantly. The full width of this peak, 2σ, is approximately 3 μm, or about half the apparent thickness of the cell layer determined visually. Thus, the cell layer thickness may be estimated from this fitting procedure to be 4σ. Additionally, the width of this peak does not shift over the nearly two-day long experiment (Fig. 3e). It is interesting that, while this peak does not broaden, it clearly grows in intensity, suggesting that secreted mucin is increasingly packed in between cells and accumulating close to the cell membrane at higher and higher concentrations. Alternatively, the diffusion and binding of Concanavalin A dye to carbohydrates in this region of the layer may be severely impeded by the lack of free space, indicating that the intensity increase within this region is diffusion limited (Fig. 3c). This observation points to potential future studies that may reveal the structural differences between the tightly bound glycocalyx right at the cell surface and the loosely bound mucin network that extends far away from the apical surface of the epithelium.

In contrast to the sharp peak at low z-locations, we find that the weaker, broad peak on the apical surface of the monolayer increases in width over time, demonstrating a thickening of the mucin layer (Fig. 3e). We plot the full width of the fitted Gaussian curve, 2σ, noting that the mucin layer can be detected up to two more standard deviations in the apical direction before the fluorescence signal begins to approach background levels. Thus, whether the layer thickness is said to vary between 18 and 24 μm or 6–8 μm, these measurements show that, in the absence of applied shear or compressive forces, secreted mucin can accumulate into structures much larger than the cell layer below.

From the fitted intensity profile at each time point, we extract the integrated intensity of the best fit Gaussian curve at higher z-locations, which is proportional to the total number of fluorophores detected in the layer of mucin sitting atop the cell monolayer. In the growth-limited regime, in which Concanavalin A/Alexa Fluor 488 conjugate arrives and binds rapidly, this number is also proportional to the total amount of mucin in the layer. Plotting the integrated fluorescence intensity of the peak at higher z-location *versus* time on a log-log scale reveals that mucin accumulates as a power-law with time, having a power close to ½; we find a best fit power of 0.58 ± 0.004. Often, when the growth of a living system is limited by the diffusive arrival of nutrients, diffusion-limited expansion occurs [21] (Fig. 3f). We will be interested in the future to use the method developed here to test whether the diffusion-limited arrival of key nutrients determine the growth kinetics of mucin layers.

4. Discussion

The combination of a thickness measurement and a proxy measurement of the integrated mass of mucin allows changes in concentration to be inferred. For example, the thickness of the mucin layer appears to increase non-monotonically throughout our experiments, exhibiting a rapid rise for 10 h, a plateau for about 12 h, then a slow rise for the remaining 20 h. In contrast to the layer thickness, the total amount of mucin appears to rise monotonically. The non-monotonic increase in mucin layer thickness combined with the monotonic increase in total amount of mucin accumulated suggests an evolving concentration in the layer; it appears that during the first 10 h of mucin production, a layer is grown at a constant concentration, while during the next 12 h the layer stops thickening and becomes more concentrated. Deeper investigation into this process will elucidate how the mucin layer protects the epithelial monolayer; combining this method with microtribometry (Pitenis et al. manuscript in this issue) or microrheological techniques will help to establish the relative roles of mucin layer thickness and mucin polymer concentration in epithelial protection. It is imminently plausible that the concentration of mucin in the cellular environment and in mucous layers will affect their rheological and tribological properties.

5. Conclusions

The technique described here provides a way to monitor changes in the spatial distribution and relative amount of mucin protein in time, while it is being produced by a living epithelial monolayer. We have identified that mucin appears to accumulate in two different spatio-temporal time-courses, with one population concentrating tightly around the cell body and another population extending very far into apical space and growing in a highly non-monotonic fashion. This method is powerful enough to distinguish between layer depth and concentration, and demonstrates that mucin production kinetics are similar to diffusion limited processes, establishing a strong hypothesis for the molecular control of mucin production and accumulation.

Acknowledgments

This work was funded by Alcon Laboratories.

References

[1] M.R. Knowles, R.C. Boucher, Mucus clearance as a primary innate defense mechanism for mammalian airways, J. Clin. Invest. 109 (2002) 571–577, http://dx.doi.org/10.1172/JCI200215217.
[2] R.A. Cone, Barrier properties of mucus, Adv. Drug Deliv. Rev. 61 (2009) 75–85, http://dx.doi.org/10.1016/j.addr.2008.09.008.
[3] J. Perez-vilar, R.L. Hill, Secreted Mucins, (n.d.).
[4] I.K. Gipson, Distribution of mucins at the ocular surface, Exp. Eye Res. 78 (2004) 379–388, http://dx.doi.org/10.1016/S0014-4835(03)00204-5.
[5] B. Yáñez-Soto, B.C. Leonard, V.K. Raghunathan, N.L. Abbott, C.J. Murphy, Effect of stratification on surface properties of corneal epithelial cells, Investig. Ophthalmol. Vis. Sci. 56 (2015) 8340–8348, http://dx.doi.org/10.1167/iovs.15-17468.
[6] P. Ramamoorthy, J.J. Nichols, Mucins in contact lens wear and dry eye conditions, Optom. Vis. Sci. 85 (2008) 631–642, http://dx.doi.org/10.1097/OPX.0b013e3181819f25.
[7] F.J. Holly, M.A. Lemp, Tear physiology and dry eyes, Surv. Ophthalmol. 22 (1977) 69–87, http://dx.doi.org/10.1016/0039-6257(77)90087-X.
[8] R.R. Hodges, D.A. Dartt, Tear film mucins: front line defenders of the ocular surface; comparison with airway and gastrointestinal tract mucins, Exp. Eye Res. 117 (2013) 62–78, http://dx.doi.org/10.1016/j.exer.2013.07.027.
[9] S.K. Lai, Y.Y. Wang, D. Wirtz, J. Hanes, Micro- and macrorheology of mucus, Adv. Drug Deliv. Rev. 61 (2009) 86–100, http://dx.doi.org/10.1016/j.addr.2008.09.012.
[10] I.K. Gipson, P. Argüeso, Role of mucins in the function of the corneal and conjunctival epithelia, Int. Rev. Cytol. 231 (2003) 1–49, http://dx.doi.org/10.1016/S0074-7696(03)31001-0.
[11] I.K. Gipson, S. Spurr-Michaud, P. Argüeso, A. Tisdale, T.F. Ng, C.L. Russo, Mucin gene expression in immortalized human corneal-limbal and conjunctival epithelial cell lines, Invest. Ophthalmol. Vis. Sci. 44 (2003) 2496–2506, http://dx.doi.org/10.1167/iovs.02-0851.
[12] R. Bansil, B.S. Turner, Mucin structure, aggregation, physiological functions and biomedical applications, Curr. Opin. Colloid Interface Sci. 11 (2006) 164–170, http://dx.doi.org/10.1016/j.cocis.2005.11.001.
[13] M.J. Waner, M. Gilchrist, M. Schindler, M. Dantus, Imaging the molecular dimensions and oligomerization of proteins at liquid/solid interfaces, J. Phys. Chem. B 5647 (1998) 1649–1657.
[14] A. Round, M. Berry, T.J. McMaster, S. Stoll, D. Gowers, A.P. Corfield, M.J. Miles, Heterogeneity and persistence length in human ocular mucins, Biophys. J. 83 (2002) 1661–1670, http://dx.doi.org/10.1016/S0006-3495(02)73934-9.
[15] M. Berry, Human preocular mucins reflect changes in surface physiology, Br. J. Ophthalmol. 88 (2004) 377–383, http://dx.doi.org/10.1136/bjo.2003.026583.
[16] I.K. Gipson, Y. Hori, P. Argüeso, Character of ocular surface mucins and their alteration in dry eye disease, Ocul. Surf. 2 (2004) 131–148, http://dx.doi.org/10.1016/S1542-0124(12)70149-0.
[17] D.M. Robertson, L. Li, S. Fisher, V.P. Pearce, J.W. Shay, W.E. Wright, H.D. Cavanagh, J.V. Jester, Characterization of growth and differentiation in a telomerase-immortalized human corneal epithelial cell line, Investig. Ophthalmol. Vis. Sci. 46 (2005) 470–478, http://dx.doi.org/10.1167/iovs.04-0528.
[18] D.B. Hill, B. Button, Mucins: Methods and Protocols, (2012), http://dx.doi.org/10.1007/978-1-61779-513-8_15.
[19] B. Sumner, Jack Bean Globulins, (1999), pp. 45–48.
[20] P. Smith, D.B. Reid, C. Environment, L. Palo, P. Alto, P.L. Smith, A Tlreshold Selection Method from Gray-Level Histograms, (1979), pp. 62–66.
[21] R. Alberty, G.G. Hammes, Application of the theory of diffusion-controlled reactions to enzyme kinetics, J. Phys. Chem. 62 (1958) 154–159, http://dx.doi.org/10.1021/j150560a005.